Nanotechnology Perceptions
ISSN 1660-6795
www.nano-ntp.com

Synthesis of Lawsonia Inermis (Henna) Carbon Supported AgO Nanocomposite, Characterizations and Photocatalytic Activity Studies

T. Sivasankar[1], R. Naveenkumar[1], B. Karthikeyan[1*], B. Vijayakumar[2]

[1]Department of chemistry, Annamalai university, Tamil Nadu, 608 002, India.
[2]Department of chemistry, Panimalar Engineering College, Tamil Nadu, 600123, India.
Email: bkarthi_au@yahoo.com

Synthesis of Carbon-supported AgO nanocomposite is reported for the first time. Henna carbon was successfully synthesized from henna leaf. Bare AgO and C-AgO nanocomposites are effectively made using the precipitation method. The synthesised composites structural, morphological, and optical properties are assessed using FT-IR, XRD, FE-SEM, UV-DRS, and PL techniques. FT-IR analysis proved that specific functional groups of synthesized materials. The uniform distribution of the composites is revealed in the FE-SEM. XRD measurements show that the materials show a cubic phase. Bandgap values are of 2.17 and 1.72 eV for AgO and C-AgO, respectively; these nanocomposites show a high degree of semiconductivity. Methylene blue (MB) dye is used as a model contaminant to quantify the composites photocatalytic activity. The photodegradation capacities of AgO, and C-AgO catalysts increased to 85.28, 95.90%. Consequently, compared to the pure AgO, the C-AgO composite performs better due to the synergetic effect of the henna carbon which boosted UV light absorption with reduce charge carrier recombination with enhanced photocatalytic activity. A possible mechanism is suggested as the carbon effect. The C-AgO nanocomposite showed a better photocatalytic activity due to the reduced bandgap, PL intensity and increasing surface area. The C-AgO nanocomposite is used for the degradation of organic pollutants in water, such as dyes, pharmaceuticals, pesticides, and industrial waste. These pollutants are broken down into harmless substances, often carbon dioxide and water, making it a green alternative for treating wastewater.

Keywords: Henna carbon, AgO, Nanocomposite, Degradation of MB dye.

1. Introduction

The field of nanotechnology is new and has shown unparalleled growth with a wide range of applications. The primary method used by this technique uses particles with a size range of 10–100 nm. Nanomaterials can be beneficial. across various sectors, including biotechnology, medicine, electronics, and medical treatment. In the field of technology, AgNPs have a prominent place among different nanoparticles, due of their affordability non-toxicity and favourable to the environment [1-4]. But textile industry's widespread discharge of waste hazardous dyes industry into aquatic bodies has sparked worries for the environment because its poisonous and detrimental effects on ecosystems and humans. Thus, it is crucial that these dyes be mineralized in order to prevent any possible dangers brought by dyes and their intermediaries. Differential Photocatalysis has been used extensively to break down the hazardous chemicals into less complex and safe products by the production of reactive species produced by semiconductor illumination [5, 6].

However, by creating metal oxide-based nanocomposite structures, these issues can be solved. Numerous composite nanomaterials based on titania, including Ag_2O/TiO_2 nanofibers, $Ag@TiO_2$ core shell structures, TiO_2/graphene, TiO_2/graphene oxide, TiO_2-carbon nanotubes (CNTs) composite nanostructures, $TiO_2/g\text{-}C_3N_4$ [6], $TiO_2(B)/Ag_2O$, ZnO/TiO_2, graphene-$ZnTiO_3$, reduced graphene oxide (r-GO)/Pd–TiO_2/r-GO , and Ag_2O/graphene oxide, have emerged as promising materials for visible light mediated photocatalysis as well as for lowering the rate of electron-hole recombination. The creation of these nanocomposites by physical and chemical processes is not energy-efficient or environmentally benign, despite the fact that they demonstrate better photocatalytic effectiveness in eliminating harmful chemicals [7]. The synthesis of Ag/ZnO nanocomposites has been reported using a number of methods thus far, including sol-gel, photoreduction, chemical deposition, hydrothermal, and pulsed laser deposition. However, because they call for high pressures, high temperatures, hazardous chemicals, pricey equipment, or lengthy synthesis times, the majority of these methods cannot be used in a commercial setting. To satisfy the demands of the economy and environment, Ag/ZnO nanocomposites require a low-cost, straightforward, and safe method. While a lot of work has been done to create Ag/ZnO nanocomposite, very little of this research has concentrated on green production techniques [8, 9].

Actually, researchers have focused a great deal of work on carbon modification or supported photocatalytic systems because it is a simpler method of suppressing the recombination of photogenerated carriers and enhancing visible light response ability [10-12].

The most promising approach, given the current state of the world and the impending environmental dangers, appears to be to use those leaves as a starting point for the production of porous carbon, which may then be reused as adsorbents, catalytic supports, and capacitor electrodes before being disposed of. Generally, either chemical activation using impregnation agents or physical activation using steam or carbon dioxide is required to make porous carbon from biomass. According to certain reports, chemical activation improves the growth of porous structures and uses considerably less energy [13-18].

In this study, we present the synthesis and characterization of AgO and C-AgO nanocomposite using the precipitation method, which is quick, inexpensive, readily

controlled, and cost-effective. The carbon source is from henna, a traditional cosmetic leaf. The material is characterized by using FT-IR, P-XRD, FE-SEM, UV-DRS, and PL analysis. The photocatalytic activity of AgO and C-AgO nanocomposite is assessed by photodegrading methylene blue (MB).

2. Experimental Methods

Materials

Henna leaves collected from the local, Henna carbon, Henna leaf extract prepared by the known method, silver nitrate ($AgNO_3$), NaOH, EtOH, Distilled water, and Whatman filter paper.

Synthesis of carbon from henna leaves

Henna leaves (Lawsonia inermis) were collected in the garden of the Annamalai University campus, then 20g of the leaves were completely cleaned with deionized water to get rid of all the dust, and they were then allowed to dry at room temperature for a week. The sample was then placed in an alumina crucible and dried for five hours at 90 ^{0}C in a vacuum oven. After three hours at 30 ^{0}C, the samples cooled spontaneously. Ultimately, carbon samples that were prepared were produced.

Extraction of henna leaf extract

To remove dirt, distilled water was used to clean fresh henna leaves several times. To achieve the proper degree of dryness, the leaves were then allowed to air dry for 5 days at room temperature. After that, a mortar and pestle were used to grind it into a fine powder. 10 grams of leaf powder and 200 mL of distilled water were combined to create the henna leaf extract, which was then boiled for 90 min at 80 ^{o}C. This solution was then allowed to cool gradually to ambient temperature, and in order to preserve it for later use, it was filtered using Whatman Grade 1 filter paper and refrigerated at 5 °C.

Synthesis of C-AgO nanocomposite

0.1M $AgNO_3$ solution was dissolved in 100 mL of distilled water and magnetically stirred for 15 min at 80 ^{o}C then added 30 mL of henna leaf extract the precipitate was obtained. Then, 0.1 M NaOH was added to enhance precipitation of dark black color, continuously stirred for 3 hours and finally, 0.05 g of henna carbon was added to stirred continuously for 1 hr. The sample was filtered, washed with ethanol and dried in an oven at 100 ^{o}C for 3 hours, finally kept in a muffle furnace for 5 hours at 500 $^\circ$ C. The same procedure follows to synthesize bare AgO nanoparticle.

Characterization studies

Cu-Kα radiation (λ = 1.5418 Å) from the X-ray system (XPERT PRO) was utilized to analyse the sample diffraction profiles. The material functional groups were assigned by the use of an FT-IR (IR Tracer-100 Shimadzu) spectrophotometer. Shimadzu UV-2600 was used to detect diffuse reflectance spectra (UV-vis DRS) between 200 and 800 nm. The sample photoluminescence emission was measured using a Perkin Elmer LS 55 fluorescence spectrometer. Using CARL ZEISS-SIGMA 300 FESEM with the EDAX FE-SEM apparatus

model, the morphology of the nanocomposites was examined.

Photocatalytic experiment

MB dye was used to examine the photocatalytic activity of the synthesised AgO and C-AgO nanocomposites. Individual photocatalytic degradation of MB was performed in 100 mL of pure water with a 0.001 M solution containing 100 mg of catalyst. In the photoreactor chamber, the solution was irradiated with UV light, and samples were taken at regular time intervals of 15 minutes. A UV-visible spectrophotometer with a wavelength range of 200 to 800 nm was used to assess the degradation samples. The absorption wavelength of MB dye was found to be 665 nm.

$$\text{Degradation Rate (\%)} = \frac{Co-Ct}{c_0} \times 100 \qquad (1)$$

where C_0 is the beginning concentration of the MB and Ct is the concentration after a time interval.

3. Results and Discussion

FT-IR analysis

The functional groups of AgO and C-AgO were investigated using Fourier transform infrared (FT-IR) spectroscopy in the 400–4000 cm^{-1} wavenumber range (Fig. 1). Fig. 1(a) displays AgO's infrared spectra. The spectrum's absorption bands at 415-524 cm^{-1} that indicate Ag-O bonds provided unambiguous proof that AgO was present. The metal-oxygen stretching frequencies are reported in the 400–600 cm^{-1} range, corresponding to the vibrations of the M–O bond, as per Fig. 1(b). The existence of physiosorbed water molecules connected to Ag nanoparticles is indicated by the absorption week bands at 3457 and 1647 cm^{-1}, respectively, which are attributed to the OH stretching and bending vibrations [19]. Moreover, the C-O-coupled stretching is responsible for the bands at 1372 cm^{-1}. The modest absorption peak that appears at 1050 cm^{-1} is caused by the OH stretching vibration of the H_2O present in the AgO lattice [20, 21]. Finally, it has been discovered that doping tends to reduce particle size, as shown by the IR band widening and expanding when AgO is exposed to additional carbon. When the particle size decreases, the system develops defects and local lattice distortions that degrade the crystal symmetry and widen the FT-IR peaks.

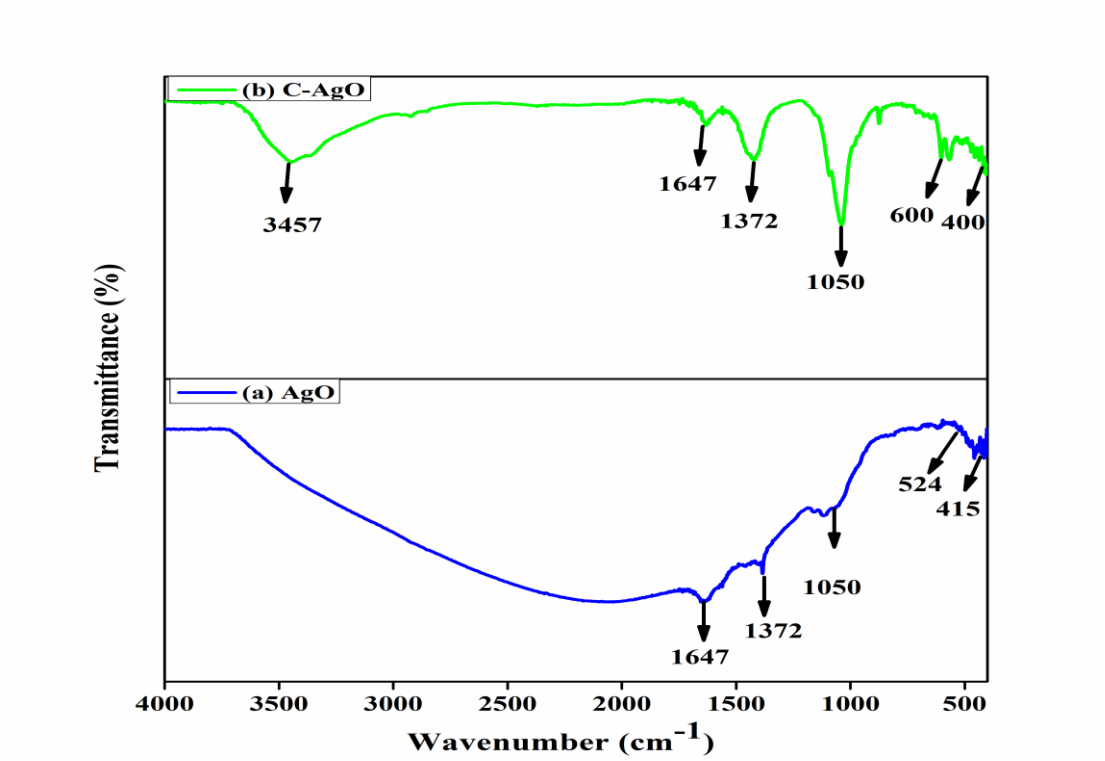

Fig.1: FT-IR Analysis of Synthesized a) Ago, b) C-Ago Nanocomposite

XRD analysis

The powder X-ray diffraction method was used to characterize the synthesized AgO and C-AgO. The AgO, C-AgO XRD pattern is displayed in Fig. 2. AgO is evident from the XRD pattern. The sample's nanocrystalline nature was validated by the XRD spectrum's broadness. The cubic phase of Ag can be identified by the four primary characteristic diffraction peaks that were found at 2θ = 38.21 (111), 44.31 (200), 64.49 (220), and 77.29 (311). (JCPDS No. 04-0783). In addition to Ag diffraction peaks, the XRD spectra also display two minor diffraction peaks at 2θ = 32.29 (202) and 46.24 (132). These two peaks, which fit well with the typical AgO JCPDS data (JCPDS No. 84-1108) [22], attest to the existence of AgO in the sample. The synthetic C-AgO sample primarily consists of AgO nanoparticles, based on the low-intensity peaks for AgO that were identified (Fig. 2). If the C-AgO, the intensity was lower. There's a chance that the carbon is amorphous or disorganized. This can result in a deficiency of identifiable peaks. The crystallite size was calculated using Debye-Scherrer equation (2)

$$D = \frac{0.98\lambda}{\beta \mathrm{Cos}\theta} \qquad (2)$$

Where λ is the X-ray beam operating system wavelength, θ is the diffraction angle, β is the full-width half maximum determined from the peak of highest intensity, and D is the crystalline size. Using equation 2 of the Debye-Scherrer formula, the average crystalline

sizes of the AgO and C-AgO nanocomposite were found to be 7.14 nm and 5.66 nm, respectively.

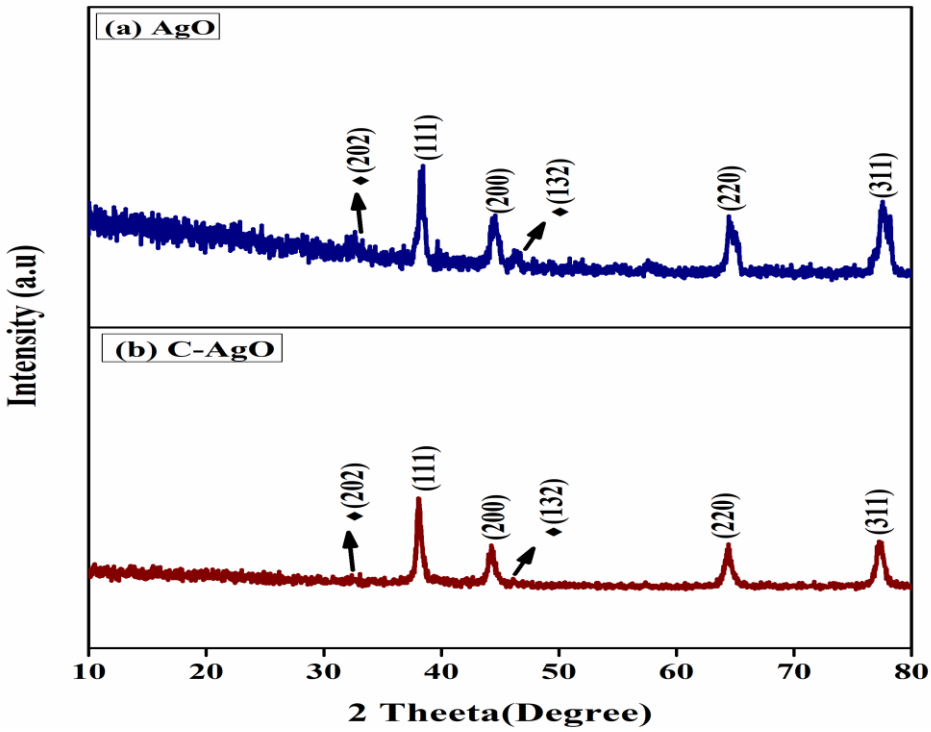

Fig. 2: XRD Pattern of a) Ago, b) C-Ago Nanocomposite

FE-SEM analysis

By using scanning electron microscopy (FE-SEM), the size, shape, morphology, and size distribution of the two samples were determined. The FE-SEM images of pure AgO and C-AgO are displayed in Fig. 3 (a and b), respectively. It appears that there are seed particles. However, upon closer inspection, we find that every nanoparticle is made up of several tiny, rigidly agglomerated nanoparticles. The agglomerated particle surface seems smoother in the FE-SEM image. The uneven, spherical-like form of nanoparticles is depicted in these images from Fig. 3(a). The carbon is evenly distributed throughout the AgO in Fig. 3(b) [23, 24]. AgO and C-AgO have average particle sizes between 52.35 and 34.28 nm, according to their morphology. Fig. 3 displays the results of energy dispersive spectroscopy (EDS) on pure AgO and C-AgO. EDS analysis verified that C-AgO is created as the study's Ag, O, and C signals are the only elements shown.

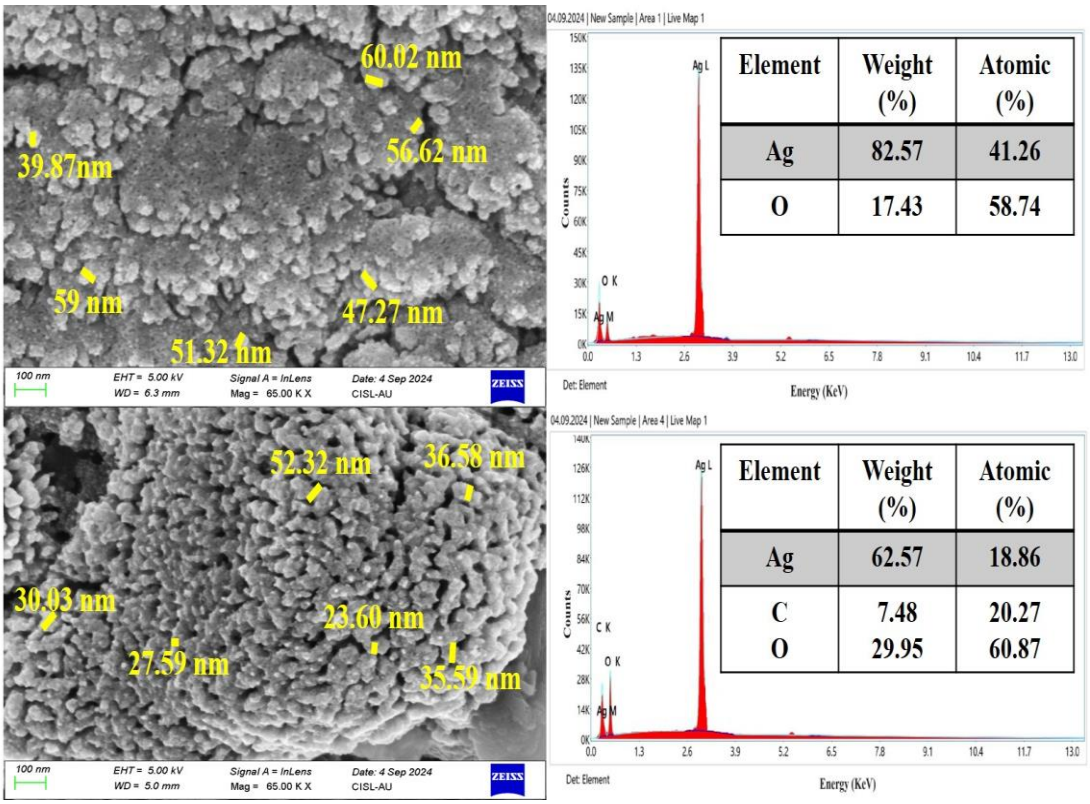

Fig. 3: FE-SEM Image of a) Ago, b) C-Ago Nanocomposite

UV-DRS Analysis

Fig. 4 displays the diffuse reflectance spectra (DRS). The wavelength range in which the optical reflectance spectra is obtained was 200–800 nm. Using the Kubelka-Munk relation equation (3) and the observed DRS spectra, we were able to determine the AgO NPs' and C-AgO's band gap energy. For all scenarios, the determined band gap energy values are 2.17 and 1.72 eV (Fig. 4).

$$\alpha h\nu = A\,(h\nu - E_g)^{1/2} \qquad (3)$$

where A is the material constant, Eg is the bandgap energy, and n = 2 is the direct energy bandgap [25-27]. Fig. 4 demonstrates unequivocally how the carbon composite in the C-AgO material causes its band gap energy to be lower than that of pure AgO. As a result, it is proposed that the reduced band gap energy of the C-AgO nanocomposite can be used to provide desirable photocatalytic activity.

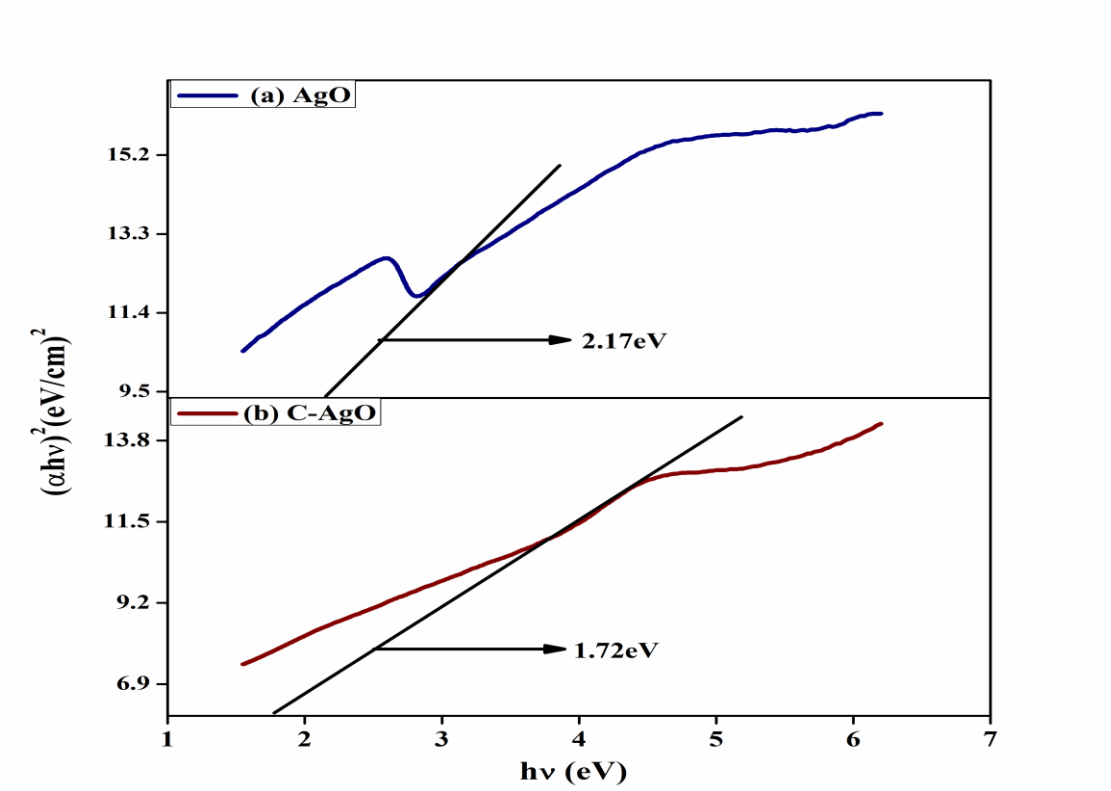

Fig .4: UV-DRS visible spectra of a) AgO, b) C-AgO nanocomposite

Photoluminescence analysis

The electrical structure and recombination process-induced loss of photogenerated electron holes in semiconductors are better understood through the use of photoluminescence (PL) spectroscopy. AgO's photoluminescence (PL) spectra at an excitation wavelength of 409 nm are displayed in Fig. 5. The C-AgO nanocomposite also had luminescent peaks at this wavelength, but its PL intensity was lower than that of the AgO. AgO's increased PL emission intensity indicates a faster rate of charge carrier recombination. Reduction of electron-hole pair recombination is implied by a decrease in photoluminescence intensity in C-AgO nanocomposites upon compositing. C-AgO nanocomposites have increased photocatalytic activity because the separated charge carriers are what drive the photocatalytic performance. In the case of C-AgO nanocomposites, band bending at the interface may be the cause of the decrease in PL intensity following the addition of carbon, leading to a very effective charge transfer process. The electrons and holes are sufficiently separated to lower the likelihood of recombination, and, as a result, the PL intensity is reduced because of the effective charge transfer mechanism. Numerous excitons are present at the AgO and C-AgO interface during UV light illumination, which could aid in achieving significant photocatalytic activity. As a result, the C-AgO nanocomposite's reduced intensity when compared to AgO shows that electron and hole recombination is inhibited and that these particles participate in photochemical transformation, which increases the nanocomposites'

photocatalytic activity. AgO/Ag2O may have fewer excited electrons forming in the compound and fewer luminous centres available, which could account for its low photoluminescence intensity. These findings concur with those published by Paul et al. [28, 29] in their investigation of AgO nanoparticles and C-AgO, whereby they noted a decrease in PL intensity on AgO-coated composite carbon.

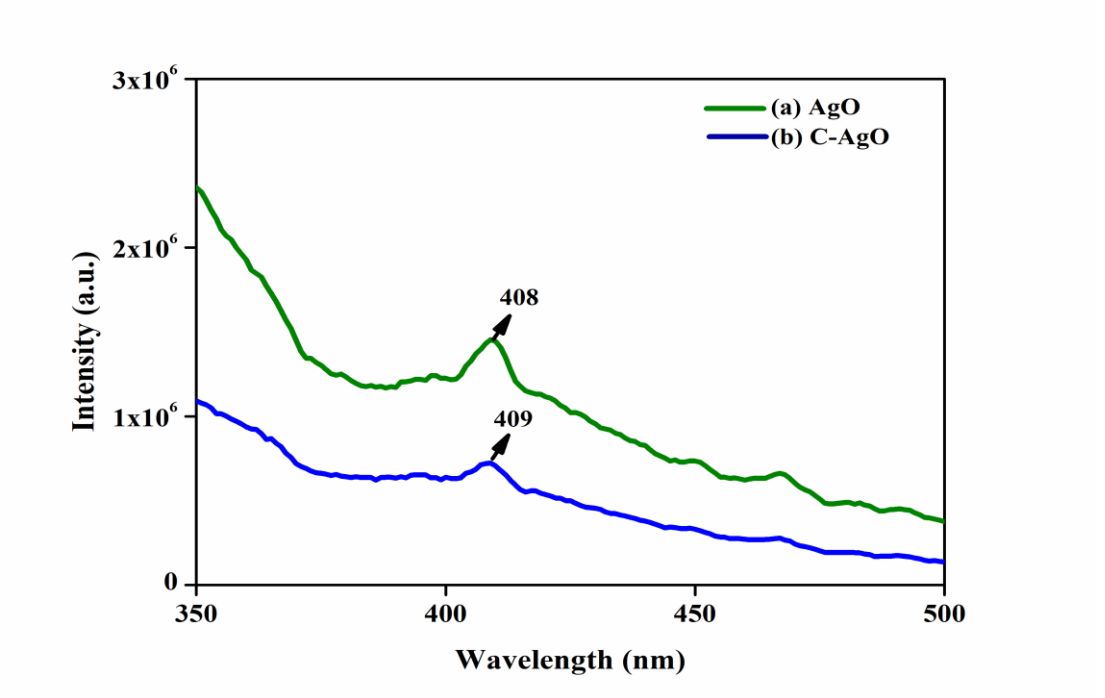

Fig .5: PL Emission Spectra of a) AgO, b) C-AgO Nanocomposite

PHOTOCATALYTIC ACTIVITY STUDIES

The capacity of the composites to eliminate MB is used to evaluate their photocatalytic activity. AgO and C-AgO nanocomposite weighing 100 mg were immersed in 100 mL of MB solution and subjected to ultraviolet radiation. Every 15 minutes, 4 mL of the MB solution are collected from the dye solution to analyze the photocatalytic activity. The measurement of MB dye absorption at a wavelength of 665 nm is depicted in Fig. 6. This is how the deterioration rate percentage was calculated using equation (1). where C_0 represents the beginning dye solution concentration (mg L^{-1}) at a certain time period and C_t represents the final dye solution concentration (mg L^{-1}).

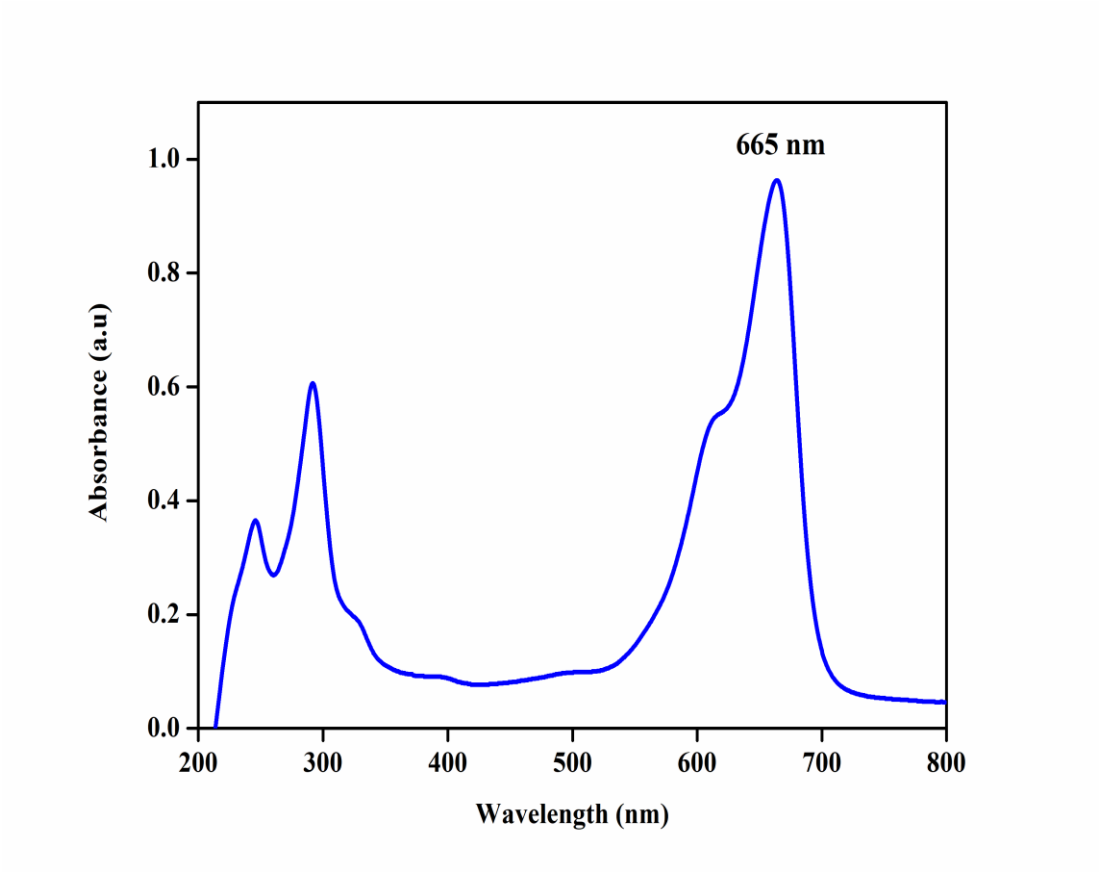

Fig .6: UV-Visible Absorption Spectrum of MB Dye

The photocatalytic activity of the synthesized AgO and C-AgO nanocomposites is shown in Fig. 7 (a, b). Compared to AgO composites, C-AgO nanocomposites exhibit substantially higher photocatalytic activity. C-AgO nanocomposites photodegrade MB dye after 15 minutes of UV light exposure. This emphasizes how crucial transparency is to MB photodegradation. As the henna carbon is added with AgO, the photocatalytic activity increases. The degradation of MB dye on the catalyst surface from 0 to 120 minutes is shown in Fig.7 (a, b). As the time interval gets longer, the MB dye concentration decreases.

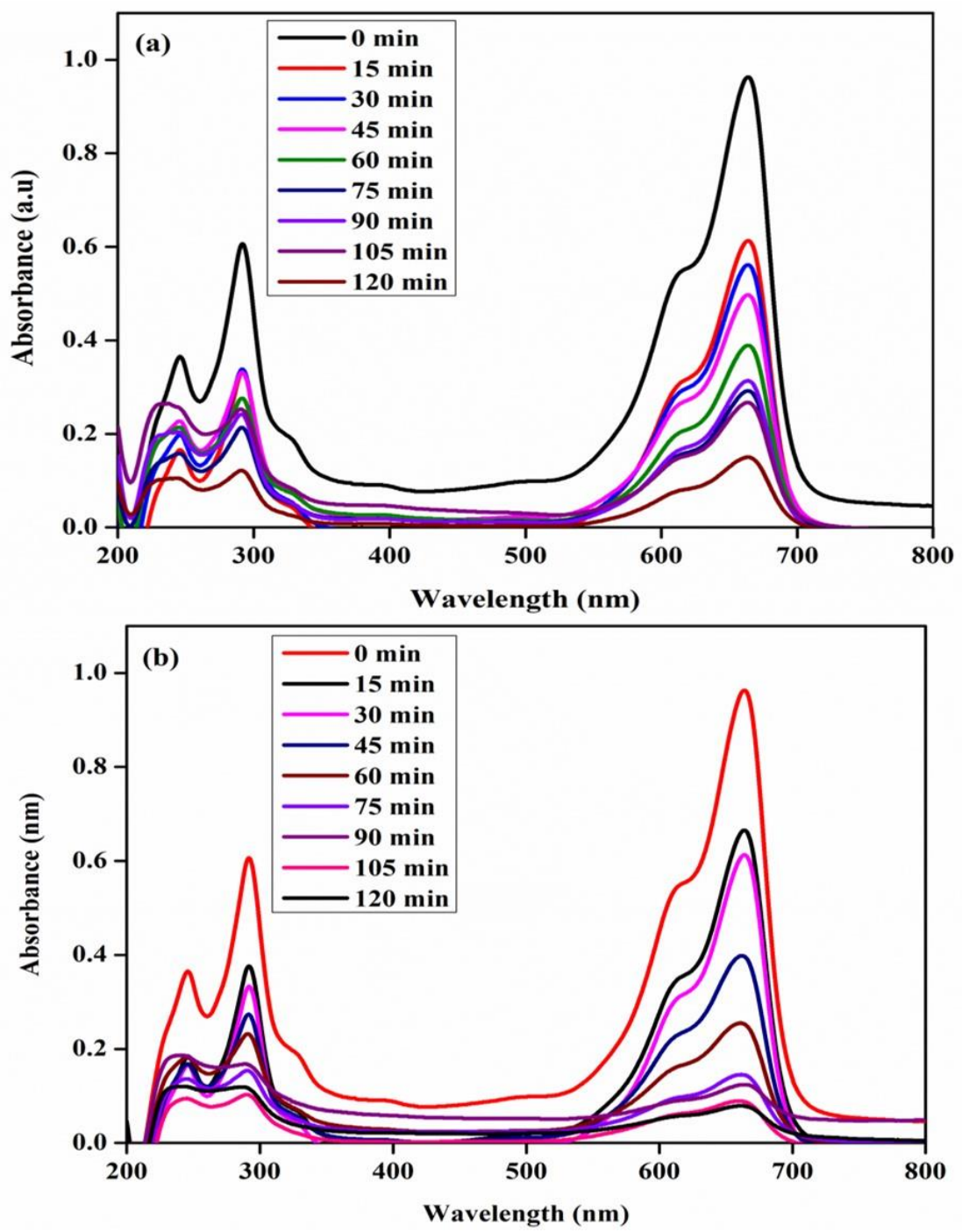

Fig .7: Photodegradation Spectrum of MB Dye Under UV-Light a) AgO, b) C-AgO Nanocomposite

The primary cause of photocatalytic degradation is explained in equation 4-9. The formation of hydroxyl radicals on the catalyst surface is a result of electrons moving from the conduction band to the valence band. A hydroxyl radical that is produced has an impact on the dye molecule's conjugation system. Moreover, the holes will react with water to produce radicals called hydroxyls (OH). As has been covered in several literatures, superoxide and radicals are the primary cause of the breakdown of dye molecules and the creation of H_2O, CO_2, and other molecules [30-33].

$$PVA/TiO_2/LF + h\nu \rightarrow e^- (TiO_2) + h^+ \quad (4)$$

$$H_2O + h^+ \rightarrow H^+ + OH \quad (5)$$

$$O_2 + e^- \rightarrow \cdot O_2^- \quad (6)$$

$$O_2^- + 2H^+ \rightarrow H_2O_2 \quad (7)$$

$$\cdot OH + MB\ Dye \rightarrow Degraded\ product \quad (8)$$

$$\cdot O_2^- + MB\ Dye \rightarrow CO_2 + H_2O \quad (9)$$

The percentage of MB dye degradation was determined in Fig. 8. The MB dye molecule's aromatic rings break down, which lowers the absorbance of the dye solution even further. While AgO only degrades MB 85.28 percent after 120 minutes of UV irradiation, the C-AgO composite degrades the dye to 95.90%. C-AgO's fast photodegradation of MB dye may be coupled with a strong ability to divide electron holes. Because electron-hole recombination is hindered by the henna carbon effect, photocatalytic activity increases. The C-AgO composite has a higher active surface area than the other samples, and it also shows more photocatalytic activity. As per the findings of their experiment, when AgO nanoparticles supported by carbon were stimulated by UV radiation, the inhibition of electron-hole pair recombination increased the activation of the active radical species, hence augmenting dye degradation.

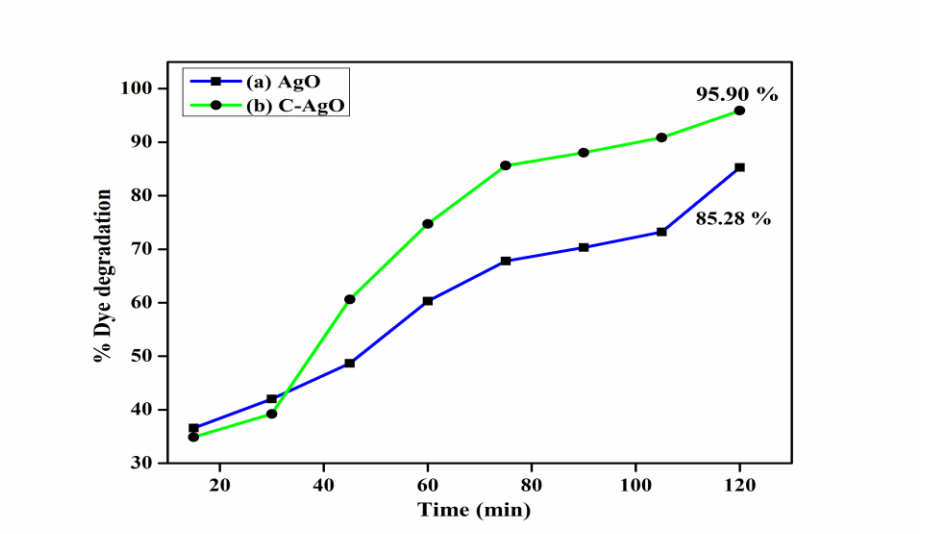

Fig.8: Degradation % of a) AgO, b) C-AgO Nanocomposites

Kinetic study

The photodegradation of MB dye using a photocatalyst often proceeds in pseudo-first order, as the equation (10) illustrates.

$$\ln (C_0/C_t) = kt \qquad (10)$$

where C_0 is the initial concentration of MB dye, Ct is the concentration of MB dye at reaction time (t), and kt is the rate constant (min). A plot of the photocatalyst samples' time-dependent UV light irradiation, photodegradation rate, and photocatalyst efficiency is shown in Fig. 9 (a & b). The plot displays the dynamic efficiency of MB dye degradation for the C-AgO nanocomposite following a pseudo-first-order request response rate.

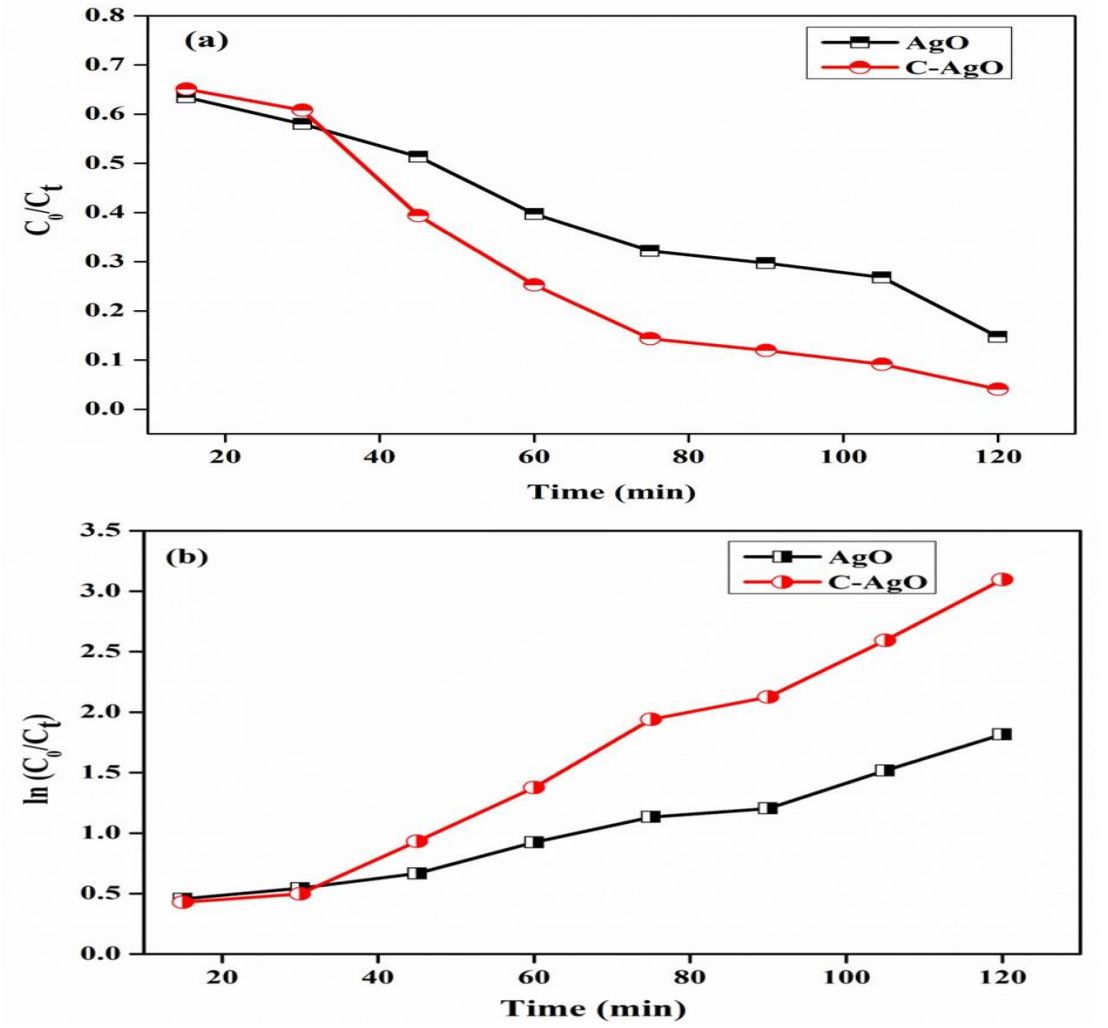

Fig .9: (a &b) Kinetic Graph of a) AgO, b) C-AgO.

The slopes of the curves' linear relationships indicate that the K values for pure AgO and C-AgO are, respectively, 0.0129 and 0.0264. AgO's and C-AgO's R^2 values are 0.9742 and

0.9854. As illustrated in Fig. 9 (a& b), the C-AgO exhibits enhanced dye degradation efficiency based on the rate constant values.

4. Conclusion

In this study, Henna carbon was successfully prepared and used to synthesize C-AgO. FT-IR, XRD, FE-SEM, UV-DRS, and PL were used to characterize the generated composites. To evaluate the composites photocatalytic activity, MB dye was utilized. The utilization of FT-IR data ascertained the properties of the composites' chemical bond structure. According to the XRD study, the materials utilized in composites have different properties. The results from the FE-SEM showed that the composites were distributed uniformly. The results of an EDS examination have determined the components of composites. AgO and C-AgO photocatalytic activity experiments showed that a MB dye degraded by 85.28% in 120 minutes, while C-AgO showed a degradation efficiency of 95.90%. It was found that henna carbon increases the efficiency of dye degradation. C-AgO material exhibits better photocatalytic properties compared to AgO. The results imply that this C-AgO nanocomposite could be helpful as potential photocatalysts for the dye pollution photodegradation process.

ACKNOWLEDGEMENT

None

AUTHOR CONTRIBUTION

T. Sivasankar contributed to collecting primary data, design the experiment, doing the experimental analysis, and overall manuscript writing and finalizing it. R. Naveen Kumar, B. Karthikeyan and B. Vijayakumar were involved in supervision, formal analysis, contributing to drafts, checking drafts, resources, and editing manuscripts and provided necessary facilities. was involved in

CONFLICT OF INTEREST STATEMENT

The authors declare no conflict of interest in this research work.

DATA AVAILABILITY STATEMENT

Manuscript has no associated data.

References

1. Sahoo M, Vishwakarma S, Panigrahi C, Kumar J. Nanotechnology: Current applications and future scope in food. Food Frontiers. 2021 Mar;2(1):3-22.
2. Varadavenkatesan T, Selvaraj R, Vinayagam R. Phyto-synthesis of silver nanoparticles from Mussaenda erythrophylla leaf extract and their application in catalytic degradation of methyl orange dye. Journal of Molecular Liquids. 2016 Sep 1; 221:1063-70.
3. Pirtarighat S, Ghannadnia M, Baghshahi S. Green synthesis of silver nanoparticles using the plant extract of Salvia spinosa grown in vitro and their antibacterial activity assessment. Journal of Nanostructure in Chemistry. 2019 Mar; 9:1-9.
4. Keat CL, Aziz A, Eid AM, Elmarzugi NA. Biosynthesis of nanoparticles and silver

nanoparticles. Bioresources and Bioprocessing. 2015 Dec; 2:1-1.
5. Bhakya S, Muthukrishnan S, Sukumaran M, Muthukumar M, Kumar ST, Rao MV. Catalytic degradation of organic dyes using synthesized silver nanoparticles: a green approach. Journal of Bioremediation & Biodegredation. 2015 Jul 1;6(5):1.
6. Silva MK, Marques RG, Machado NR, Santos OA. Evaluation of Nb2O5 and Ag/Nb2O5 in the photocatalytic degradation of dyes from textile industries. Brazilian Journal of Chemical Engineering. 2002; 19:359-63.
7. Kulal D, Kodialbail VS. Visible light mediated photocatalytic dye degradation using Ag2O/AgO-TiO2 nanocomposite synthesized by extracellular bacterial mediated synthesis-An eco-friendly approach for pollution abatement. Journal of Environmental Chemical Engineering. 2021 Aug 1;9(4):105389.
8. Sun F, Qiao X, Tan F, Wang W, Qiu X. One-step microwave synthesis of Ag/ZnO nanocomposites with enhanced photocatalytic performance. Journal of Materials Science. 2012 Oct; 47:7262-8.
9. Sun Y, Zhao Z, Li G, Li P, Zhang W, Han Z, Lian K, Hu J. Synthesis and characterization of Ag@ ZnO nanostructures for photocatalytic degradation of rhodamine B: influence of calcination temperature and Ag content. Applied Physics A. 2017 Feb; 123:1-9.
10. Yin C, Zhu S, Chen Z, Zhang W, Gu J, Zhang D. One step fabrication of C-doped BiVO 4 with hierarchical structures for a high-performance photocatalyst under visible light irradiation. Journal of Materials Chemistry A. 2013;1(29):8367-78.
11. Niu M, Zhu R, Tian F, Song K, Cao G, Ouyang F. The effects of precursors and loading of carbon on the photocatalytic activity of C–BiVO4 for the degradation of high concentrations of phenol under visible light irradiation. catalysis Today. 2015 Dec 1; 258:585-94.
12. Tang J, Song B, Deng Q, Xin H. Facile hydrothermal-carbonization approach to carbon-modified BiVO4 composites with enhanced photocatalytic activity. Materials Science in Semiconductor Processing. 2015 Jul 1; 35:90-5.
13. Sun L, Tian C, Li M, Meng X, Wang L, Wang R, Yin J, Fu H. From coconut shell to porous graphene-like nanosheets for high-power supercapacitors. Journal of materials Chemistry A. 2013;1(21):6462-70.
14. Biswal M, Banerjee A, Deo M, Ogale S. From dead leaves to high energy density supercapacitors. Energy & Environmental Science. 2013;6(4):1249-59.
15. Yu M, Han Y, Li J, Wang L. CO2-activated porous carbon derived from cattail biomass for removal of malachite green dye and application as supercapacitors. Chemical Engineering Journal. 2017 Jun 1; 317:493-502.
16. Sudaryanto Y, Hartono SÁ, Irawaty W, Hindarso H, Ismadji S. High surface area activated carbon prepared from cassava peel by chemical activation. Bioresource technology. 2006 Mar 1;97(5):734-9.
17. Taha A, Ben Aissa M, Da'na E. Green synthesis of an activated carbon-supported Ag and ZnO nanocomposite for photocatalytic degradation and its antibacterial activities. Molecules. 2020 Mar 30;25(7):1586.
18. Shahshahanipour M, Rezaei B, Ensafi AA, Etemadifar Z. An ancient plant for the synthesis of a novel carbon dot and its applications as an antibacterial agent and probe for sensing of an anti-cancer drug. Materials Science and Engineering: C. 2019 May 1;98:826-33.
19. Hosseinpour-Mashkani SM, Ramezani M. Silver and silver oxide nanoparticles: Synthesis and characterization by thermal decomposition. Materials Letters. 2014 Sep 1;130:259-62.
20. Sobhani-Nasab A, Behpour M. Synthesis and characterization of AgO nanostructures by precipitation method and its photocatalyst application. Journal of Materials Science: Materials in Electronics. 2016 Feb;27:1191-6.
21. Waterhouse GI, Bowmaker GA, Metson JB. The thermal decomposition of silver (I, III) oxide: A combined XRD, FT-IR and Raman spectroscopic study. Physical Chemistry Chemical

Physics. 2001;3(17):3838-45.
22. Gauri B, Vidya K, Sharada D, Shobha W. Synthesis and characterization of Ag/AgO nanoparticles as alcohol sensor. Res J Chem Environ. 2016 Oct;20(10):1-5.
23. Mohammadi M, Hekmatara SH, Moghaddam RS, Darehkordi A. Preparation and optimization photocatalytic activity of polymer-grafted Ag@ AgO core-shell quantum dots. Environmental Science and Pollution Research. 2019 May 1;26(13):13401-9.
24. Petkova GA, Záruba K, Žvátora P, Král V. Gold and silver nanoparticles for biomolecule immobilization and enzymatic catalysis. Nanoscale research letters. 2012 Dec; 7:1-0.
25. Mohanaparameswari S, Balachandramohan M, Sasikumar P, Rajeevgandhi C, Vimalan M, Pugazhendhi S, Ganesh Kumar K, Albukhaty S, Sulaiman GM, Abomughaid MM, Abu-Alghayth M. Investigation of structural properties and antibacterial activity of AgO nanoparticle extract from Solanum nigrum/Mentha leaf extracts by green synthesis method. Green Processing and Synthesis. 2023 Nov 1;12(1):20230080.
26. Rita A, Sivakumar A, Dhas SS, Dhas SM. Structural, optical and magnetic properties of silver oxide (AgO) nanoparticles at shocked conditions. Journal of Nanostructure in Chemistry. 2020 Dec; 10:309-16.
27. Sobhani-Nasab A, Behpour M. Synthesis and characterization of AgO nanostructures by precipitation method and its photocatalyst application. Journal of Materials Science: Materials in Electronics. 2016 Feb; 27:1191-6.
28. Shetty V. Solar light active biogenic titanium dioxide embedded silver oxide (AgO/Ag2O@ TiO2) nanocomposite structures for dye degradation by photocatalysis. Materials Science in Semiconductor Processing. 2021 Sep 1; 132:105923.
29. Balraj B, Arulmozhi M, Siva C, Krithikadevi R. Synthesis, characterization and electrochemical analysis of hydrothermal synthesized AgO incorporated ZrO2 nanostructures. Journal of Materials Science: Materials in Electronics. 2017 Apr; 28:5906-12.
30. Naveenkumar R, Karthikeyan B, Senthilvelan S. Synthesis of bioinspired lotus fiber infused PVA/TiO2 nanocomposites: characterization, thermal, and photocatalytic activity studies. Biomass Conversion and Biorefinery. 2023 Dec 26:1-3.
31. Naveenkumar R, Karthikeyan B, Senthilvelan S. Facile Green Synthesis of Activated Biocarbon-Cobalt-Doped TiO2 Nanocomposite for Enhanced Antibacterial Effect and Efficient Photocatalytic for Dye Degradation. Brazilian Journal of Physics. 2024 Oct;54(5):170.
32. Naveenkumar R, Karthikeyan B, Senthilvelan S. Photocatalytic Degradation of Toxic Rhodamine B Dye by Green-Synthesised Activated Carbon-Supported Cobalt Doped ZnO With Further Assessment of ZnO Nanoparticles in Antimicrobial Applications. ChemistrySelect. 2024 Aug 5;9(29): e202401448.
33. Vijayakumar, B., & Karthikeyan, B. (2022). Synthesis and characterization of CdO-SnO2 NPs with excellent performance for Naphthol Blue Black (NBB) dye photodegradation and multi-application study. Materials Today: Proceedings, 67, 128–136.